

Implementation of a Current Linear Regulator Based on a GaN HEMT for Laser Diode Manipulations

Kai-Jun Pai¹ and Chang-Hua Lin²

¹ Undergraduate Program of Vehicle and Energy Engineering, National Taiwan Normal University, Taiwan (R.O.C.)

² Department of Electrical Engineering, National Taiwan University of Science and Technology, Taiwan (R.O.C.)

Abstract-- In this study, a gallium nitride (GaN) high electron mobility transistor (HEMT) combined with the operational amplifier was applied to develop a two-level linear regulator (TLLR). Using the TLLR, the operating current of the laser diode can be formed in the constant-current or pulse-width modulation mode to emit the continuous-wave or short-pulsed laser, respectively. When the operating current of the laser diode was operated at the high-frequency PWM, the parasitic elements on the GaN HEMT, laser diodes, print-circuit board (PCB), and power wires influence the rising-edge slope of the laser operating current. In accordance with the physical packages of the GaN HEMT and laser diode, their equivalent circuit model parameters were provided in this study; therefore, the TLLR simulation circuit with its parasitic element was established. The simulation and experiment waveforms can be obtained to confirm the developed TLLR.

Index Terms-- Gallium nitride, high electron mobility transistor, linear regulator, laser diode, continuous-wave short-pulsed.

I. INTRODUCTION

In recent years, semiconductor devices have developed three generations. Silicon (Si) and germanium (Ge) were used as the based semiconductor materials, they are the semiconductor devices of the first generation. In the second generation, the chemical compounds were composed of two elements, such as gallium arsenide (GaAs) and indium phosphide (InP). In the third generation, the chemical compounds of the wide band gap materials are used, such as the gallium nitride (GaN) and silicon carbide (SiC); the GaN transistors are based on the GaN-on-SiC or GaN-on-Si. Using GaN transistors, the switching frequency and temperature can be higher than the traditional Si transistors; thus, the semiconductor materials of the third generation have been used in electric vehicles, industrial productions, and 5th generation (5G) communication systems.

GaN elements can produce the two-dimensional electron gas (2DEG) on the material face, their switching frequency can be high than the conventional Si-based element. The high electron-mobility is the 2DEG characteristic, it can promote electronic conduction in the lateral GaN. However, the electrical connection of the lateral configuration element is situated at the same plane surface of the active element, and the lateral configuration results in a low withstand voltage; thus, the lateral configuration elements are more commonly applied in the

GaN elements with a withstand voltage below 600 V. The electrical connection of the vertical GaN and active element are respectively situated at the top and bottom sides of the semiconductor configuration, hence the 2DEG cannot form to promote electron mobility; thus, the vertical GaN element characteristic approximates the SiC, and it can be applied in the GaN device with a high withstand voltage which is greater than 900 V. [1]–[5].

Reviewed for previous literature, the light-emitting diode (LED) is incorporated with the liner regulator for its driving current control [6]–[9]. In [6], [7], the MOSFET was used; in [8], [9], the bipolar junction transistors (BJT) was used; only in [10], the GaN HEMT was used in the linear regulator. Moreover, the dimming function used the PWM technology in [6]–[9], and the PWM frequency was lower than 2-kHz.

In this study, both PWM and continuous constant-current technologies were used to adjust the optical output power of the laser diode (LD), the PWM frequency and short-pulsed time can be set at 200-kHz and 1-μs, respectively.

II. EQUIVALENT CIRCUIT MODEL

When the laser diodes and GaN HEMTs are operated at the high-frequency, the device's intrinsic parasitic elements must be considered, because the operating frequency and parasitic element values influence the circuit characteristic. The package, electrical parameter, and equivalent circuit model (ECM) for the use of laser diode and GaN HEMT in the study explain in the following.

A. LD ECM

The model number of the laser diode is PL TB405B (Osram Opto Semiconductors Inc.), its specifications are list as follows [11]:

- Package: TO-52.
- Emission wavelength: 450-nm.
- Operating temperature: −40 to 85 °C.
- Optical output power: 1.6-W.
- Maximum operating current: 1.5-A.

The package model number of the laser diode was the TO-52, and the ECM with parasitic element based on the TO-52 package is shown in Fig. 1. In Fig. 1(a), the laser diode included the two metal terminals (T_{ld_an} and T_{ld_ca}), p - and n -type contacts, bonding wires, active layer, and substrate. The power source inputs the two metal

terminals, the bonding wires connect the *p*- and *n*-type contacts with the active layer and substrate, respectively.

The ECM based on the TO-52 package (Fig. 1(a)) is shown in Fig. 1(b). The equivalent circuit included the package and chip parasitic elements. The package parasitic elements included the extracted submount capacitor C_{pld} , bonding wire inductor L_{pld} , and bonding wire resistor R_{pld} . The chip parasitic elements included the chip electrode capacitor C_{cpld} , chip resistor R_{cpld} , and intrinsic diode D_{cpld} [12]–[15]. From Figs. 1(a) and 1(b), C_{pld} was between the *p*- and *n*-type contacts, L_{pld} and R_{pld} were on the bonding wires. The chip electrodes formed the C_{cpld} . The R_{cpld} represented the chip parasitic resistor. The D_{cpld} represented the diode characteristic of the laser diode.

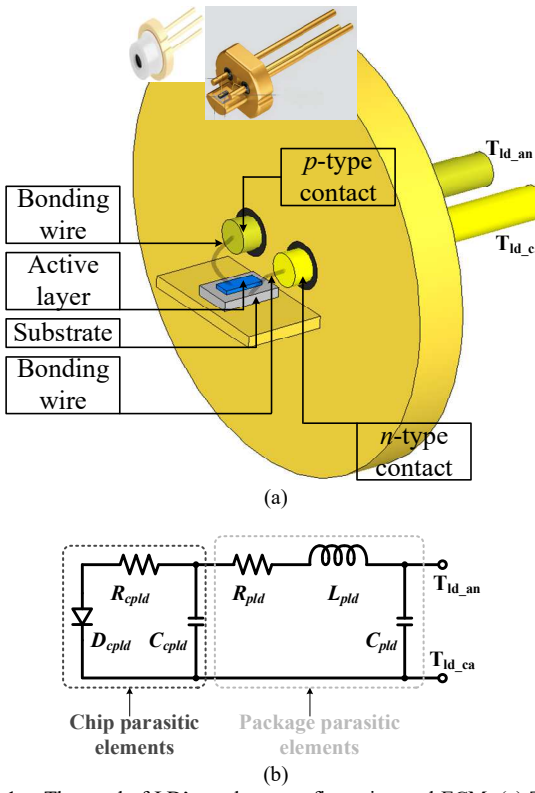


Fig. 1. The used of LD's package configuration and ECM. (a) TO-52 package; (b) ECM. (Modified from [16]–[18].)

B. GaN HEMT ECM

The model number of the GaN HEMT device is GS61004B (GaN systems Inc.), its specifications are list as follows [19]:

- Package: GaN_{PX} package.
- Drain–source withstand voltage: 100-V.
- Drain–source turning on resistor: 16-mΩ.
- Gate-to-source threshold voltage: 1.7-V.
- Internal gate resistor: 0.9-Ω.
- Input capacitor (C_{iss}): 260-pF.
- Output capacitor (C_{oss}): 110-pF.
- Reverse transfer capacitor (C_{rss}): 5-pF.

The package configuration and ECM of the GaN HEMT were shown in Fig. 2. The GS61004B was the flat no-lead package which was designed by GaN systems Inc. This package configuration can reduce the intrinsic parasitic

inductor. The 3-dimention (3D) chip configuration and package was illustrated in Fig. 2(a). The GS61004B chip included the substrate, Si substrate, GaN buffer layer, 2DEG channel, aluminum GaN (AlGaN) buffer layer, *p*-GaN contact, gate (G), drain (D), source (S) electrodes, bottom-side of chip package, and contact pad [19]–[22]. The 2-dimention (2D) semiconductor configuration was illustrated in Fig. 2(b).

The ECM of the GaN HEMT has the extrinsic and intrinsic elements [23]–[26], as shown in Fig. 2(c). The intrinsic elements includ the resistors (R_{gs} and R_{ds}), capacitor C_{ds} , dependent current source $g_m \times v_g$; the g_m represented the transconductance, the v_g is a voltage across C_{gs} . The extrinsic elements includ the inductors (L_{pd} , L_{pg} , and L_{ps}), capacitors (C_{pd} and C_{pg}), and resistors (R_{pd} , R_{pg} , and R_{ps}).

The pad connection, electrode, and across capacitor formed C_{pd} and C_{pg} . The contact resistor and semiconductor bulk resistor are R_{pd} , R_{pg} , and R_{ps} . The gate, source, and drain terminals of the GaN HEMT incorporating contact pads of the bottom-side of chip packages can form the parasitic resistors (R_{pd} , R_{pg} , and R_{ps}) and inductors (L_{pd} , L_{pg} , and L_{ps}).

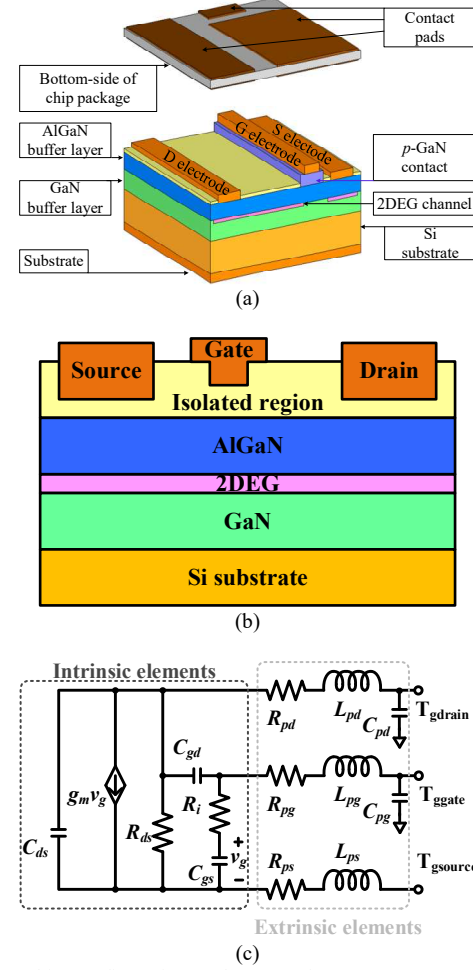


Fig. 2. Chip configuration and ECM of GaN HEMT. (a) 3-D chip configuration; (b) 2-D semiconductor configuration; (c) ECM. (Modified from [16], [17].)

In Fig. 2(c), the intrinsic elements with the gate

electrode and drain-source channel can form the parallel-plate capacitor C_{gs} , the p -GaN contact was the dielectric of C_{gs} . C_{ds} and C_{gd} are the equivalent capacitors, because the drain and source electrodes are constructed on the 2DEG. Finally, the drain-source terminal has a channel resistor R_{ds} .

III. TLLR BASED ON GAN HEMT

The circuit block diagram of the TLLR based on the GaN HEMT is shown in Fig. 3, including the microcontroller unit (MCU), voltage buffer, integral circuit, operational amplifier (OPA), GaN HEMT, current buffer, current detection resistor (R_{cs}), differential amplifier (DA), and current-sink switch (CSS), CSS driver, and laser diodes (LD_1 – LD_3).

Both pulse-width modulation (PWM) signals (PWM_{amp} and PWM_{pul}) are from the MCU's PWM ports. PWM_{amp} inputs to the integral circuit, an average (direct-current) voltage can be obtained, the voltage buffer can prevent load effect. The voltage buffer outputs a reference current command ($I_{ld(ref)}$) for the TLLR; therefore, the TLLR can compare the $I_{ld(ref)}$ with the DA output voltage (V_{da}) to control the GaN HEMT operation. The current buffer can promote the instantaneous driving current of the OPA output terminal for the GaN HEMT fast turning on. Therefore, the LD_1 – LD_3 can be driven by a continues constant-current using the TLLR.

The TLLR was composed of the OPA, current buffer, GaN HEMT, current detection resistor R_{cs} , and DA. The equivalent resistor of the drain-source terminal of the GaN HEMT can be adjusted to control the laser diode current I_{ld} . Moreover, the frequency of PWM_{pul} must be increased to accomplish the short-pulsed current; however, increasing PWM_{pul} frequency, the bandwidth of elements including the OPA, current buffer, and DA must be greater than PWM_{pul} frequency. Furthermore, the OPA output current is insufficient, hence the gate-source capacitor C_{gs} cannot be fast charged to turn on the GaN HEMT; for this reason, the current buffer is used to promote the OPA output current.

The CSS driver can be used to promote the driving ability of PWM_{pul} , and it can output a voltage signal V_{css} to control the CSS turning on/off, and further to control the GaN HEMT. The CSS can be controlled by V_{css} ; when V_{css} is the high-voltage level, the CSS switch is turned on; in this condition, the CSS can form a current sink to draw the current from the gate terminal of the GaN HEMT; as a result, the gate voltage of the GaN HEMT was reduced to be lower than the GaN HEMT threshold voltage, hence the GaN HEMT can be turned off. When V_{css} was the low-voltage level, the CSS was turned off, no current drew to CSS, the gate voltage of the GaN HEMT can increase to be higher than the GaN HEMT threshold voltage, hence the GaN HEMT can be turned on to regulate I_{ld} .

From Fig. 3, the operating timing of the TLLR is shown Fig. 4, and explained as follows:

t₀ to t₁: When PWM_{pul} is at the zero-voltage mode, the CSS was turned off. Using the integral circuit and voltage buffer, PWM_{amp} forms an average voltage $I_{ld(ref)}$ as a reference current command to control the driving current

I_{ld} . Meanwhile, the laser diodes are operated in the forward-bias, and I_{ld} is the continues constant-current.

t₁ to t₂: When PWM_{pul} is the PWM mode operation, the CSS can be controlled following the PWM state for the turning-on or -off operations. When PWM_{pul} is the high-voltage level in the PWM mode, the CSS can be turned on, hence the sink current of the CSS results in the GaN HEMT turning off, and then no current can drive the laser diodes.

t₂ to t₃: PWM_{pul} is the PWM mode operation. When PWM_{pul} was the low-voltage level of the PWM mode, the CSS can be turned off, hence the sink current of the CSS is disable resulting in the GaN HEMT turning on, hence the gate voltage of the GaN HEMT can be controlled by the OPA output voltage. Meanwhile, the laser diodes are operated in the forward-bias, and I_{ld} is the continues constant-current.

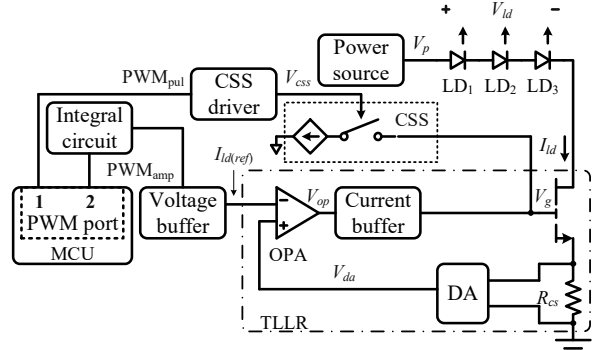


Fig. 3. Circuit block diagram of the TLLR. (Modified from [16], [17].)

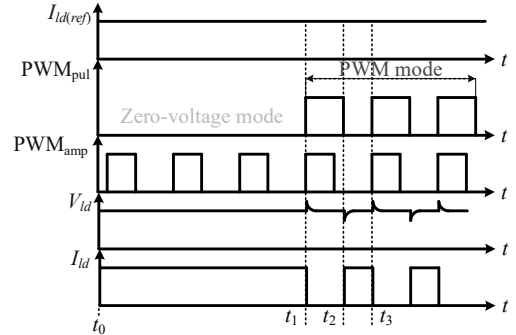


Fig. 4. Operating timing of TLLR. (Modified from [16], [17].)

A. TLLR Specification

- Forward bias, V_{ld} : 5 to 6-V.
- Operating current, I_{ld} : 0 to 1.2-A.
- Driving power source, V_p : 15-V.
- PWM signal, V_{pwm_pul} : 5-V, 0 to 100%, 200-kHz.
- PWM signal, V_{pwm_amp} : 5-V, 0 to 100%, 10-kHz.
- Current reference command, $I_{ld(ref)}$: 0 to 1.2-V.

B. Simulation Circuit & Parameter Calculation

From the circuit block diagram in Fig. 3, the circuit simulation software PSIM (Powersim Inc., Rockville, United States) was used, the block diagram of the simulation circuit is shown in Fig. 5.

In the GaN HEMT ECM, the parasitic wire inductors and resistors on the print circuit board (PCB) were considered, including the (L_{pcb1} and L_{pcb2}) and (R_{pcb1} and

R_{pcb2}) between in the T_{gen_g} to CSS, and the T_{gen_g} to the current buffer, respectively. The L_{pcb3} and R_{pcb3} was between in the T_{gen_s} and R_{cs} . The L_{pcb4} and R_{pcb4} was between in the T_{gen_d} and the third LD ECM of the cathode terminal (T_{ld_ca}).

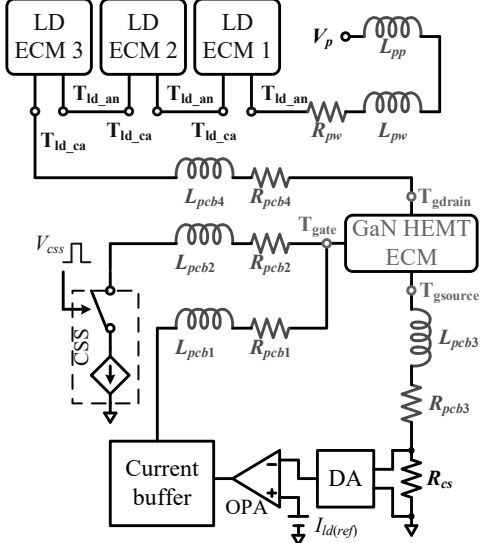


Fig. 5. Simulation circuit block diagram. (Modified from [16], [17].)

The parasitic wire inductor and resistor on the power cable of the power source (V_{cc}) were considered. The parasitic wire inductor (L_{pw}) and resistor (R_{pw}) were on the PCB, the parasitic inductor from the V_{cc} was the L_{pp} . The L_{pw} , R_{pw} , and L_{pp} were connected in series between in the V_{cc} and the anode terminal (T_{ld_an}) of the first LD ECM.

C. LD ECM and GaN HEMT Parameters

Literatures [13]–[15] were referred and the worst case values were used for these parameter values. In Fig. 1(b), the LD ECM parameters list in Table I [16], [17].

In Fig. 2(c), the element parameters list in Table II [16], [17].

TABLE I
LD ECM PARAMETERS IN FIG. 1(B)

Reference	[13]	[14]	[15]	This study
Symbol				
C_{cpld}	13 pF	10.2 pF	10.2 pF	20 pF
R_{cpld}	4.2 Ω	4.3 Ω	4.3 Ω	1 Ω
V_{fb}	X	X	X	5 V
C_{pla}	0.77 pF	0.067 pF	0.066 pF	1 pF
L_{pla}	300 pH	280 pH	280 pH	1 nH
R_{pla}	2 Ω	2 Ω	2 Ω	2 Ω

'X' represents a situation that was undescribed.

0

TABLE II
ELEMENT PARAMETER VALUES IN FIG. 2(C)

Symbol	Value	Symbol	Value
L_{pd}	100 pH	C_{pd}	1 pF
L_{pg}	100 pH	C_{pg}	1 pF
L_{ps}	100 pH	g_m	22 (A/V)
R_{gs}	0.9 Ω	R_{pd}	1 m Ω
R_{ds}	27 m Ω	R_{pg}	1 m Ω
C_{gs}	295 pF	R_{ps}	1 m Ω
C_{gd}	6.2 pF	C_{ds}	134 pF

In practical applications, the power wire $l_w = 20\text{-cm}$, d

= 0.2-cm; $L_{pw} = 210\text{-nH}$, and $R_{pw} = 2.7\text{-m}\Omega$. Moreover, the parasitic inductor L_{pp} inside the V_{cc} was consider, the $L_{pp} = 1500\text{ nH}$ was used for simulation.

D. Simulation

According to Fig. 5 and using the PSIM and, the simulation circuit can be illustrated in Fig. 6(a), the simulation results presented in Figs. 6(b) and 6(c). In Figs. 6(b) and 6(c), PWM_{pul} represented the CSS control signal, the V_g represented the gate voltage of the GaN HEMT, the I_{ld} represented the LD driving current. When PWM_{pul} was the low-voltage level, the V_g was the high-voltage level to turn on the GaN HEMT, hence the LD can be operated in the forward bias resulting in I_{ld} increase.

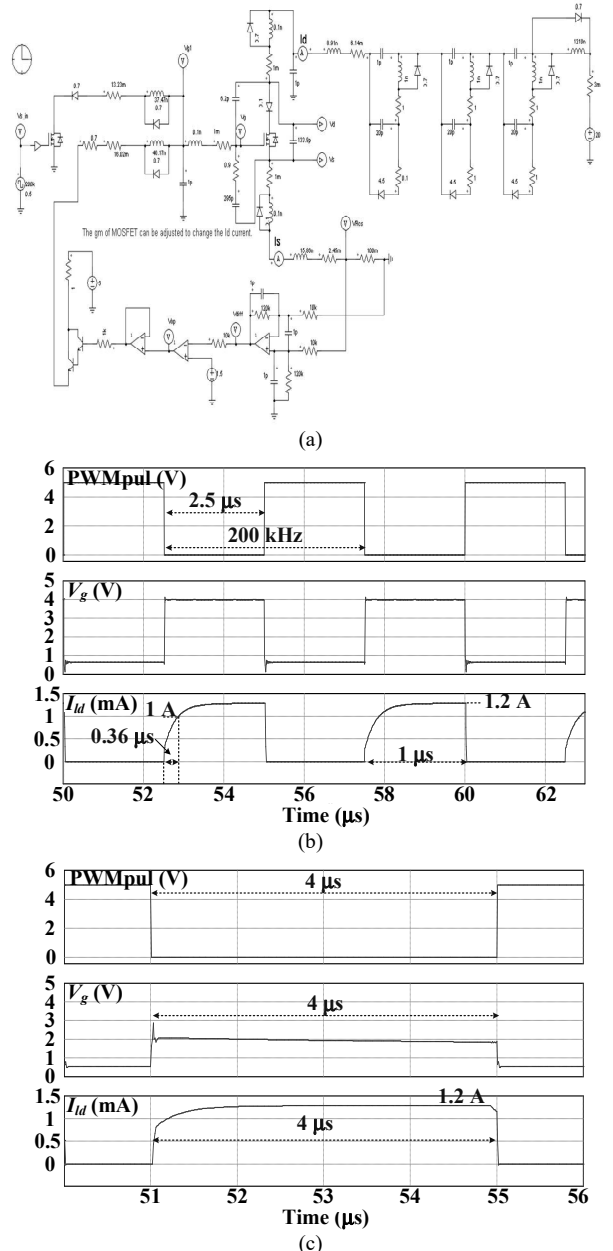


Fig. 6. TLLR simulation and pulsed time adjustment. (a) Simulation circuit schematic; (b) 2.5- μs ; (c) 4- μs . (Modified from [16], [17].)

In Fig. 6(b), the PWM_{pul} frequency was set at 200-kHz, its PWM duty cycle was set at 2.5- μs , the peak voltage of

V_g can be maintained at 4-V, the I_{ld} spent 0.36- μ s to 1-A, and spent 1 μ s to the rated current 1.2-A. In Fig. 6(c), the PWM duty cycle was adjusted to 4- μ s, the peak voltage of V_g was maintained at 2-V, the I_{ld} can be maintained in the rated current 1.2-A.

IV. EXPERIMENTAL RESULT

When the PWM_{pul} was no PWM signal, the CSS can be turned off, the gate voltage of the GaN HEMT was about 3 V, the I_{ld} can be maintained at the continuous constant-current of 1.2 A, as shown in Fig. 7.

In Fig. 8(a), the PWM duty cycle of PWM_{pul} was 0.2 (1 μ s / 5 μ s). When the PWM_{pul} was the high-voltage level, the CSS can be turned on, and then the V_g was the low-voltage level about 1 V (simulation was 0.7-V), which was low than the threshold voltage of 1.7-V, hence the I_{ld} was 0. When the PWM_{pul} was the low-voltage level, the CSS can be turned off, and then the V_g was the high-voltage level, which was equal to 4-V (simulation was 4-V), hence the I_{ld} was increased from 0 to 1-A spending 0.4- μ s (simulation was 0.363- μ s); the I_{ld} was increased from 0 to 1.2-A spending 1- μ s (simulation was 1- μ s). It was noticeable that the V_g had an offset voltage about 0.7-V, which was caused by the cut-in voltage of the CSS. In Fig. 8(b), the PWM duty cycle of PWM_{pul} was 0.76 (3.8- μ s / 5- μ s). The I_{ld} can be increased from 0 to 1.2-A.

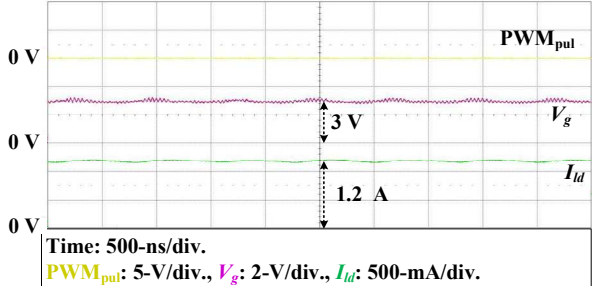
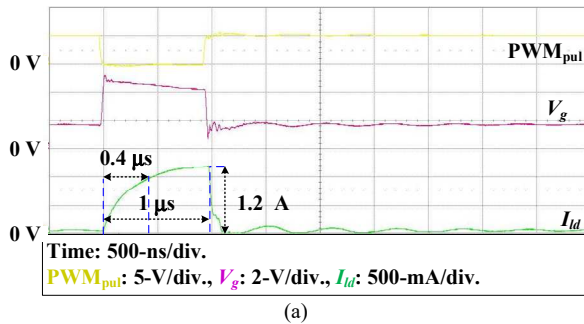
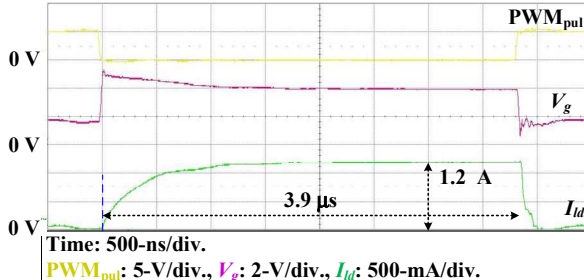


Fig. 7. Continuous constant-current operation. (Modified from [16], [17].)



(a)



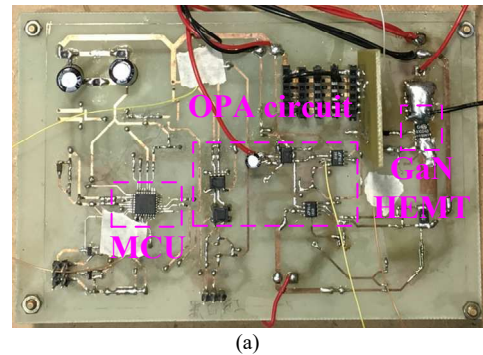
(b)

Fig. 8. Experimental waveforms, when the pulsed time of PWM_{pul} was adjusted at: (a) 20%; (b) 76%. (Modified from [16], [17].)

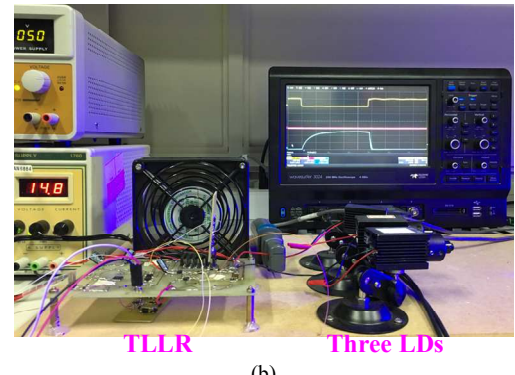
The TLLR prototype driving the three LDs presented in Fig. 9. In Fig. 9(a), it was the TLLR prototype, the MCU, GaN HEMT, and OP circuit. The three LDs were controlled by the TLLR, as shown in Fig. 9(b).

V. CONCLUSIONS

A TLLR incorporating the GaN HEMT with the wide bandwidth operational amplifier was developed and implemented. Using the TLLR, LDs was operated in both short-pulsed and continuous constant-current modes to fulfill the short-pulsed and continue-wave lasers. According to the practical packages of the laser diode and GaN device, the intrinsic parasitic elements, PCB parasitic elements, and wire inductors and resistors on power wires were considered to established a simulation circuit, and described parameter calculations in detail; thus, the critical operating waveform of the TLLR were simulated. Using the TLLR prototype, the experimental measurements were achieved to compare with the simulation waveform.



(a)



(b)

Fig. 9. A TLLR prototype driving LDs. (a) TLLR prototype; (b) TLLR and three LDs implementation.

ACKNOWLEDGMENT

Author acknowledges the National Science and Technology Council, Taiwan (R.O.C.) supporting a research fund. The grant numbers: MOST 111-2221-E-003-005 and 108-2221-E-003-028-MY2.

REFERENCES

- [1] R. Yadav and A. Dutta, "A new charge-based analytical Model for the gate current in GaN HEMTs," *IEEE Transactions on Electron Devices*, vol. 69, no. 4, pp. 2210–2213, 2022.
- [2] I. Berdalovic, M. Poljak, and T. Suligoj, "Theoretical prediction of mobility improvement in GaN-based HEMTs at high carrier densities," *IEEE Transactions on Electron Devices*, vol. 70, no. 3, pp. 1425–1429, 2023.
- [3] L. Hoffmann, C. Gautier, S. Lefebvre, and F. Costa, "Optimization of the driver of GaN power transistors through measurement of their thermal behavior," *IEEE Trans. on Power Electronics*, vol. 29, no. 5, pp. 2359–2366, 2014.
- [4] R. Reiner, P. Waltereit, B. Weiss, S. Moench, M. Wespel, S. Müller, R. Quay, and O. Ambacher, "Monolithically integrated power circuits in high-voltage GaN-on-Si heterojunction technology," *IET Power Electronics*, vol. 11, no. 4, pp. 681–688, 2017.
- [5] T. Kim, M. Jang, and V. Agelidis, "Ultra-fast MHz range driving circuit for SiC MOSFET using frequency multiplier with eGaN FET," *IET Power Electronics*, vol. 9, no. 10, pp. 2085–2094, 2016.
- [6] L. Lohaus, A. Rossius, S. Dietrich, R. Wunderlich, and S. Heinen, "A dimmable LED driver with resistive DAC feedback control for adaptive voltage regulation," *IEEE Trans. Industry Application*, vol. 51, no. 4, pp. 3254–3262, 2015.
- [7] P. Liu, Y. Hsu, and S. Hsu, "Drain-voltage balance and phase-shifted PWM control schemes for high-efficiency parallel-string dimmable LED drivers," *IEEE Trans. Industrial Electronics*, vol. 65, no. 8, pp. 6168–6176, 2018.
- [8] M. Meraj, S. Rahman, A. Iqbal, and L. Ben-Brahim, "High brightness and high voltage dimmable LED driver for advanced lighting system," *IEEE Access*, vol. 7, pp. 95643–95652, 2019.
- [9] H. Martinez and A. Saberkari, "Linear-assisted DC/DC regulator-based current source for LED drivers," *Electronics letters*, vol. 52, No. 6, pp. 437–439, 2020.
- [10] T. Lin and C. Hsia, "Integrated linear regulator for GaN-based gate driver applications," in Proc. *International Future Energy Electronics Conference (IFEEC)*, DOI: 10.1109/IFEEC47410.2019.9015137, 25–28 Nov. 2019.
- [11] OSRAM Opto Semi. Inc., "Visible laser diodes," *Datasheet of OSRAM Opto Semi. Inc.*, 2017.
- [12] N. Zhu, C. Chen, E. Pun, and P. Chung, "Extraction of intrinsic response from s-parameters of laser diodes," *IEEE Photonics Letters*, vol. 17, no. 4, pp. 744–746, Apr. 2005.
- [13] C. Chen, N. Zhu, S. Zhang, and Y. Liu, "Characterization of parasitics in to-packaged high-speed laser modules," *IEEE Trans. Advanced packaging*, vol. 30, no. 1, pp. 97–103, 2007.
- [14] M. Majewski and D. Novak, "Method for characterization of Intrinsic and extrinsic components of semiconductor laser diode circuit model," *IEEE Microwave and guided wave letters*, vol. 1, no. 9, pp. 246–248, 1991.
- [15] S. Zhang, N. Zhu, Y. Liu, and Y. Liu, "Characterization of parasitics from scattering parameters of laser diode," *Microwave and Optical Technology Letters*, vol. 50, no. 1, pp. 1–4, 2008.
- [16] K. Pai, "Employing simplified resistance-inductance-capacitance equivalent circuits to analyze and confirm a gallium nitride-based current linear regulator for laser diode controls," *International Journal of Circuit Theory and Applications*, vol. 50, no. 11, pp. 3788–3810, 2022.
- [17] K. Pai and C. Lin, "Simulation and implementation of a two-mode-operation transconductance regulator with a Gallium Nitride High-Electron-Mobility Transistor," *International Journal of Circuit Theory and Applications*, vol. 50, no. 1, pp. 197–213, 2021.
- [18] Ams-OSRAM, "ams OSRAM Metal Can® PLPT5 Blue Laser Diodes," GaNPower International Inc., March 2023. [Online]. Available: <https://www.mouser.tw/new/ams-osram/osram-plpt5-blue-laser-diodes/>
- [19] GaN systems Inc., "GS61004B 100V enhancement mode GaN transistor," *Datasheet of GaN systems Inc.*, 2020.
- [20] P. Cova, N. Delmonte, and D. Santoro, "Power GaN FET boards thermal and electromagnetic optimization by FE modeling," *Microelectronics Reliability*, vol. 100–101, pp. 1–7, 2019.
- [21] GaN systems Inc., "An introduction to GaN enhancement-mode HEMTs," *Application Note of GaN systems Inc.*, 2020.
- [22] Y. Fu, "GaN power HEMT tutorial: GaN basics," GaNPower International Inc., Oct. 2019. [Online]. Available: <http://docplayer.net/164349663-Gan-power-hemt-tutorial-gan-basics.html>
- [23] R. Essaadali, A. Jarndal, A. Kouki, and F. Ghannouchi, "A new GaN HEMT equivalent circuit modeling technique based on x-parameters," *IEEE Trans. Microwave Theory and Techniques*, vol. 64, no. 9, pp. 2758–2777, 2016.
- [24] G. Avolio, A. Raffo, I. Angelov, G. Crupi, Alina Caddemi, G. Vannini, and D. Schreurs, "Small-versus large-signal extraction of charge models of microwave FETs," *IEEE Trans. Microwave Wireless Components Letters*, vol. 24, no. 6, pp. 394–396, 2014.
- [25] I. Angelov, H. Zirath, and N. Rorsman, "A new empirical nonlinear model for HEMT and MESFET devices," *IEEE Trans. Microwave Theory and Techniques*, vol. 40, no. 12, pp. 2258–2266, 1992.
- [26] G. Dambrine, A. Cappy, F. Heliodore, and E. Playez, "A new method for determining the FET small-signal equivalent circuit," *IEEE Trans. Microwave Theory and Techniques*, vol. 36, no. 7, pp. 1151–2266, 1988.